Branched nanotrees with immobilized acetylcholine esterase for nanobiosensor applications

2010 Nanotechnology 21 055102

(http://iopscience.iop.org/0957-4484/21/5/055102)

Nanotechnology **21** (2010) 055102 (8pp) doi:10.1088/0957-4484/21/5/055102

Branched nanotrees with immobilized acetylcholine esterase for nanobiosensor applications

Klas Risveden[1], Kimberly A Dick[2], Sunil Bhand[1,3], Patrik Rydberg[4], Lars Samuelson[2] and Bengt Danielsson[1]

[1] Department of Pure and Applied Biochemistry, Center for Chemistry and Chemical Engineering, Lund University, PO Box 124, SE-22100 Lund, Sweden
[2] Solid State Physics, Lund University, Box 118, S-22100 Lund, Sweden
[3] Department of Chemistry, Birla Institute of Technology and Science-Pilani, Goa Campus, Goa 403726, India
[4] Department of Medicinal Chemistry, Faculty of Pharmaceutical Sciences, University of Copenhagen, Universitetsparken 2, DK-2100 Copenhagen, Denmark

E-mail: Kimberly.Dick@ftf.lth.se

Received 16 September 2009, in final form 25 November 2009
Published 21 December 2009
Online at stacks.iop.org/Nano/21/055102

Abstract

A novel lab-on-a-chip nanotree enzyme reactor is demonstrated for the detection of acetylcholine. The reactors are intended for use in the RISFET (regional ion sensitive field effect transistor) nanosensor, and are constructed from gold-tipped branched nanorod structures grown on SiN_x-covered wafers. Two different reactors are shown: one with simple, one-dimensional nanorods and one with branched nanorod structures (nanotrees). Significantly higher enzymatic activity is found for the nanotree reactors than for the nanorod reactors, most likely due to the increased gold surface area and thereby higher enzyme binding capacity. A theoretical calculation is included to show how the enzyme kinetics and hence the sensitivity can be influenced and increased by the control of electrical fields in relation to the active sites of enzymes in an electronic biosensor. The possible effects of electrical fields employed in the RISFET on the function of acetylcholine esterase is investigated using quantum chemical methods, which show that the small electric field strengths used are unlikely to affect enzyme kinetics. Acetylcholine esterase activity is determined using choline oxidase and peroxidase by measuring the amount of choline formed using the chemiluminescent luminol reaction.

(Some figures in this article are in colour only in the electronic version)

A biosensor is a compact analytical device incorporating a biological or biologically-derived sensing element, either integrated within or intimately associated with a physico-chemical transducer. The usual aim of a biosensor, as defined by Newman and co-workers, is to produce either discrete or continuous analog or digital electronic signals that are proportional to a single analyte or a related group of analytes [1]. In 1996 it was demonstrated that micromachining and semiconductor technology can be merged for fabrication of integrated multianalyte thermal biosensors for simultaneous detection of glucose, urea and penicillin [2]. A variety of mini- and microsensors was proposed, including thermistor-based microbiosensors, thermopile-based microbiosensors, plastic chip sensors, and microcolumn sensors [3]. The introduction of microbiosensors decreased the time of analysis, the waste of reagents and the size of the devices [4]. The further miniaturization of biosensors has received increasing attention during the last decade [5–9]. Nanobiosensors and nanoscale sensor devices have the potential for low cost, mass production of lab-on-chip systems, as well as the integration of sensor array systems for handling small sample volumes, for instance for single cell or single protein characterization with high throughput capacity [10–18].

In 2005 a new type of bioelectronic nanosensor was demonstrated for gluconate and glucose [19]. Based on

its sensing properties the device was termed a regional ion sensitive field effect transistor nanosensor, or more simply a RISFET. Scaling issues, such as the influence of the size of the sensing electrode gap, as well as the importance of using regional electric fields orthogonal to nanosensor surfaces for enhanced sensitivity, were demonstrated for glucose measurements (μM detection range) [20, 21] using RISFETs with low signal frequencies. Enhanced sensitivity has been achieved in other types of nanosensors using regional electric fields [22, 23]. The size dependence of nanosensor devices has also been addressed at high sensor signal frequencies using admittance spectroscopy [24, 25]. The influence of the signal current frequency on the organocarbamate detection sensitivity (pM detection range for carbofuran) for RISFET sensors has further been demonstrated using a 65 nm sensor gap [26]. RISFET devices can be used for many different applications [27] and the setup was recently used to show that a green fluorescent protein produced by the jellyfish *Aequorea Victoria* offers a promising strategy for the development of biophotovoltaic nanodevices [28]. In order to facilitate convenient liquid and sample application as well as simple user-friendly analysis, the RISFET has also been combined with an automatic flow injection analysis system and a novel sequential batch analysis system for continuous monitoring of nerve toxic pesticides, such as carbofuran [27] in beverages.

Semiconductor nanorods (also known as nanowires) represent a promising framework for nanoscale applications, and the field has developed very rapidly in the last 5–10 years [29, 30]. In this paper, we report a novel lab-on-a-chip reactor which uses branched nanorod structures—nanotrees—for efficient immobilization of the reacting enzymes. By placing the epitaxially-grown nanostructures in the sensing electrode gap of a RISFET [21] a nanobiosensor can be realized. The sensing range of a bioelectronic RISFET sensor benefits from keeping the conducting properties of the sensor gap high in relation to the internal resistance of the entire sensor circuit [27]. Thus, using nonconducting nanorods as a support material to lift the active surface from the chip surface above the conducting channel in between the sensing electrodes helps to prevent short-circuiting of the sensing electrode gap.

The nanotrees are grown using gold nanoparticle seeds, such that the particles remain at the tips of the branches after growth. The biological sensing elements are immobilized, as 'leaves', onto the gold surface through thiol linkage either directly or indirectly using biotin–streptavidin linkage [31]. The nanostructures can be designed to locate the sensing elements just above the conducting channel of the RISFET. The products of the biochemical reaction are then subsequently pulled down to the conducting channel by the electrical field of the RISFET, as earlier described [21, 27]. In a bioelectronic RISFET nanosensor, relatively strong electrical fields are used to increase the sensitivity. Therefore a theoretical study of the influence of an external electrical field on the activation energy of acetylcholine esterase has been included to show how the enzyme kinetics, and hence the sensitivity, can be influenced and increased by the control of electrical fields in relation to the active sites of enzymes in an electronic biosensor.

The resulting bioelectronic nanosensor uses a RISFET as a physicochemical transducer combined with epitaxially-grown low-conducting GaP nanorods or branched nanorod structures (nanotrees), which carry the biological sensing elements in the sensor electrode gap. The construction of conducting nanorod and nanotree structures using InAs would also be possible for other types of nanosensor applications.

1. Results and discussion

GaP nanorods grow epitaxially on crystalline substrates, preferentially in the $\langle 111 \rangle B$ direction (figure 1(a)) [32]. When growth is performed on GaP $\langle 111 \rangle B$ substrates, the only available growth direction is vertical from the substrates. Substrates with other alignments (for example $\langle 001 \rangle$) will give different preferential orientations with respect to the substrate; however the growth directions are always $\langle 111 \rangle B$. The use of non-polar substrates, such as Si $\langle 111 \rangle$, will result in four equivalent preferential directions, only one of which is vertical on the substrate. However, appropriate tuning of growth parameters can give preferential vertical growth on Si as well [33]. Branches growing on first-generation nanorods also adopt $\langle 111 \rangle B$ growth directions (figure 1(b)) [34]. In this case there are three equivalent directions available, all downwards at an angle of 109° to the original rod. The occurrence of stacking faults in the growth direction in the first-generation rod will result in two possible orientations of the preferential growth directions of branches, allowing for six possible $\langle 111 \rangle B$ growth directions downwards from the original rod.

Growth on non-crystalline or highly mismatched substrates does not allow for an epitaxial relationship between the nanorods and the substrate to determine the growth direction. This was observed when growing GaP nanotrees on a SiN substrate (figure 1(c)). Since there is no relationship between these two materials, the initial orientations of the GaP nuclei will be random. Following nucleation, growth will proceed in a $\langle 111 \rangle B$ direction, randomly oriented with respect to the substrate. For many applications, this random orientation is not a problem. The growth of branches on randomly-oriented GaP nanorods will still follow the available $\langle 111 \rangle B$ direction with respect to the original rod (figure 1(d)).

The GaP structures fabricated on SiN_x layers were tested, as nanoreactors, for biochemical functionality by immobilization of the enzyme AcChE. AcChE was attached to the gold part of the nanotrees by thiol chemistry, as described in section 3. As control experiments, a set of samples was non-specifically functionalized through direct adsorption of AcChE, while a different set of thiolated but not activated samples was also tested (see section 3). The reactors in turn were connected to the microwell of a 384 well plate. The reaction was initiated by addition of an acetylcholine substrate to the enzymatic nanoreactor. The substrate was allowed to react with enzyme for a sufficient time (optimized to 10 min). The choline produced was transferred to the microwell reactor. The chemiluminescent signal generated from the coupled enzymatic reaction was monitored in real time using a Peltier cooled CCD camera for measurement

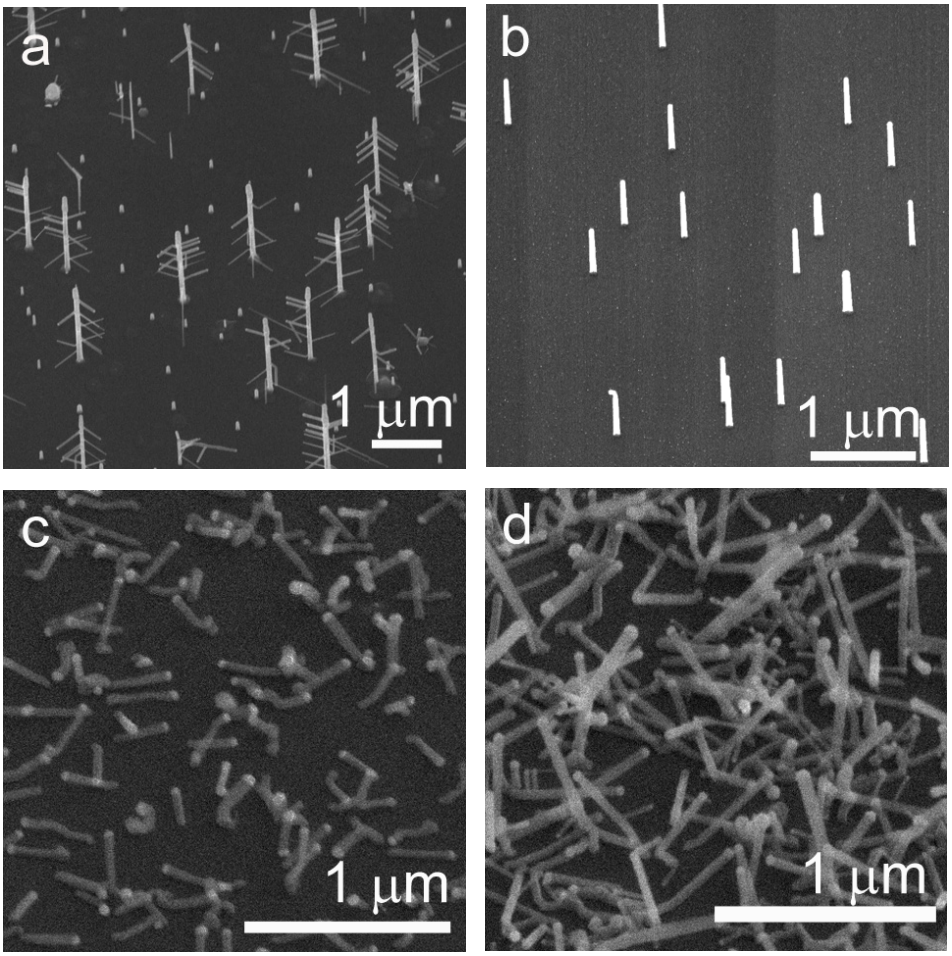

Figure 1. SEM image of GaP nanostructures. (a) 500 (length = ι) × 40 nm (diameter = θ), nanorods on a GaP substrate, tilted 45° to the surface normal, the scale bar is 500 nm. (b) Nano-'forest' of nanotrees; trunk 1500 (ι) × 40 (θ) nm, branches 300 (ι) × 20 (θ) nm, on a GaP substrate, tilted 45° to the surface normal, the scale bar is 500 nm. (c) 500 (ι) × 40 (θ) nm nanorods on a SiN_x layer, tilted 60° to the surface normal, the scale bar is 500 nm. (d) Nano-'forest' of nanotrees; trunk: 500 nm (ι) × 40 (θ) nm, branches 40 (ι) × 20 (θ) nm, on a SiN_x layer, tilted 60° to the surface normal, the scale bar is 500 nm. For all samples, and (d), the growth temperature was 440 °C and a molar fraction of 7.8×10^{-6} of trimethylgallium, and 7.5×10^{-3} of phosphine (PH_3) respectively was used. The growth time for first-generation rods in (b) was 120 s, and in (a), (c), and (d) was 60 s, while the branch growth time in (b) and (d) was 30 s.

of acetylcholine. The kinetic intensity profile of the signal generated from the production of choline was recorded. The results of the intensity profile are presented as figure 2, along with the kinetic image profile (inset, figure 2).

These kinetic intensities of the resulting signal reached a stable value after 15 min from the start of the chemiluminescence reaction. The intensities, after the stable signal was attained, were found to be almost double in the case of AcChE-functionalized nanotrees compared to the nanorods. The maximum intensities observed were: 3900 ADU for AcChE functionalized on nanotrees, 1800 ADU for AcChE functionalized on nanorods, and ADU 1300 for non-specifically adsorbed AcChE on nanotrees and nanorods respectively. Control samples thiolated but not EDC-activated (see section 3) also failed to show an intensity comparable to the above activated samples. This clearly shows that the thiol immobilization method effectively binds the active AcChE to the gold surface, and that it is most effective for the nanotrees. It is reasonable to assume that the enhanced binding observed for the nanotree sample is due to the much higher surface area available.

The nanorod structures used in the biosensors were grown in random directions on wafer materials commonly used as supports for electrode structures. As demonstrated above, such nanotrees are quick and straightforward to produce. The random directions are caused by the polycrystallinity of the material used. However, for some applications it may be advantageous to achieve vertically-oriented nanorod structures, which requires monocrystalline wafer materials. This poses a problem since many monocrystalline materials are conducting, and hence would short-circuit any electrode structures lying on the wafer. For such applications nanorods and branched nanotrees can be grown on semi-insulating, single crystalline substrates of, for instance, InP or GaAs, which are readily available. However, for the present work, vertically-oriented nanorods are not necessary to demonstrate the concept of nanorod-based lab-on-a-chip reactors.

The time required to fabricate a complete sensor chip, including both electrode structures and enzyme reactors, is considerable, so an immobilization method that allows for a quick and convenient exchange of the enzymes is desirable. In

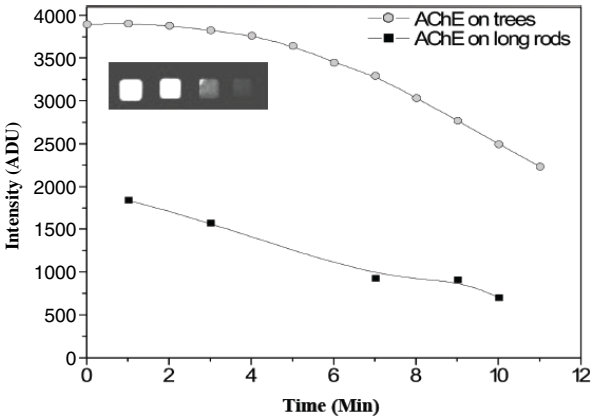

Figure 2. The comparative dynamic intensity profile for choline analyzed in micro-reactors using chemiluminescence detection (inset image) from AcChE bound to thiol-functionalized nanotrees (–O–), and AcChE bound to thiol-functionalized nanorods (–■–) measured with a CCD camera in luminescence mode.

this way, the same device could be reused when the activity of the enzymes has decreased too much for practical use or when another enzyme is required for the analyses of different target analytes. The gold caps of the nanorod structure tips allow for thiol-coupling to proteins on gold surfaces as shown here. Immobilization of target sensing enzymes to the gold caps can also be realized through thiol-coupling of target-enzyme sensitive proteins, such as streptavidin (for permanent immobilization of target enzymes), or alternatively through thiol-coupling of different kinds of lectins [36, 37] (for easily reversible immobilization of target enzymes).

The RISFET sensor is based on the principle of focusing charged reaction products with an electrical field in the region between the sensing electrodes [21, 26], creating a sample-specific conducting channel. Quantum chemical calculations (as described in section 3) showed that field strengths larger than 10 MV m^{-1} may have significant effects on the reaction rates. This effect could be used to optimize the sensitivity of electrical biosensors (including RISFET nanobiosensors, see figure 3) with enzymatic reactions by increasing the activity of the enzymes. Thus, for optimal performance of such an electrical biosensor, simulations of the electrical fields and alignment of the enzymes during immobilization may offer an additional way to optimize the sensor.

When choosing higher field strengths than 10 MV m^{-1}, perpendicular nanorods (in combination with orientational chemistry) would open up the possibility of aligning the sensing elements at any desired distance from the chip surface. This may allow for precise control of the electrical field strength for optimum activation energy, and hence maximized sensitivity of the biosensor. In a bioelectronic RISFET biosensor a special effort made on the 3D construction of an enzymatic reactor will potentially allow for optimal sensitivity.

The enzyme molecules in the vicinity of the sensing electrodes of a bioelectronic RISFET sensor are surrounded by an electrical field. In earlier reports on bioelectronic RISFET sensors [26] electrical fields of up to 0.8 MV m^{-1} over the sensing electrodes have been used. Carbofuran detection

Table 1. The maximum change of the reaction barrier for different field strengths in the range of 1–1000 MV m^{-1}.

Field strength (MV m^{-1})	Maximum change of the reaction barrier (kJ mol^{-1})
1	±0.031
10	±0.31
100	±3.1
1000	±31

is based on the ability to inhibit the enzyme acetylcholine esterase (AcChE). To estimate the effect of an electrical field on the AcChE-catalyzed reaction in a RISFET biosensor, quantum chemical calculations were performed.

The reaction studied describes the binding of the Ser-200 oxygen to the reacting carbon atom of the substrate. The product state of this reaction is not the final product in the reaction, but it is the first intermediate and it has been shown that this step in the reaction is the rate-limiting step [44]. Single point energy calculations were performed for all states in the reaction (reactant, transition state, and product), with electric fields in the x, y or z directions at a field strength of 10 MV m^{-1}, to determine the field direction which gives the largest effect on the energies. For the optimal direction (an x and y combination, as shown by the arrow in figure 4) final energies were evaluated at field strengths from 1 to 1000 MV m^{-1}. The maximum change of the reaction barrier for the different field strengths are shown in table 1. The barrier without an electric field was found to be 50 kJ mol^{-1}.

Since these calculations employ only a single configuration of the enzyme active site and do not include the surrounding protein, they will produce energy changes which are most likely higher than in reality. Thus, these data clearly show that field strengths of ca 1 MV m^{-1} will most likely not have any effect on the reactivity of the enzyme.

2. Conclusions

In this paper we characterize a novel nanotree nanoreactor that could potentially replace micro-reactors currently used in nanobiosensor applications.

Nanorod structures were grown on thermally oxidized heavily n-doped Si wafers, onto which SiN_x was deposited through chemical vapor deposition. Two different nanorod-based reactors were created: one with single nanorod structures, and one with branched nanotree structures. Acetylcholine esterase (AcChE) was immobilized on the gold-capped tips of the structures using thiol chemistry. The reactors were tested for AcChE activity of the analyte acetylcholine chloride through secondary chemiluminescence measurements. Significantly higher activity was found for the nanotree-based reactors as compared to the nanorod reactors, most likely due to increased surface area of the dendritic nanotree structure.

The possible effects of electrical fields in RISFET nanosensor devices on the function of acetylcholine esterase were investigated using quantum chemical methods which

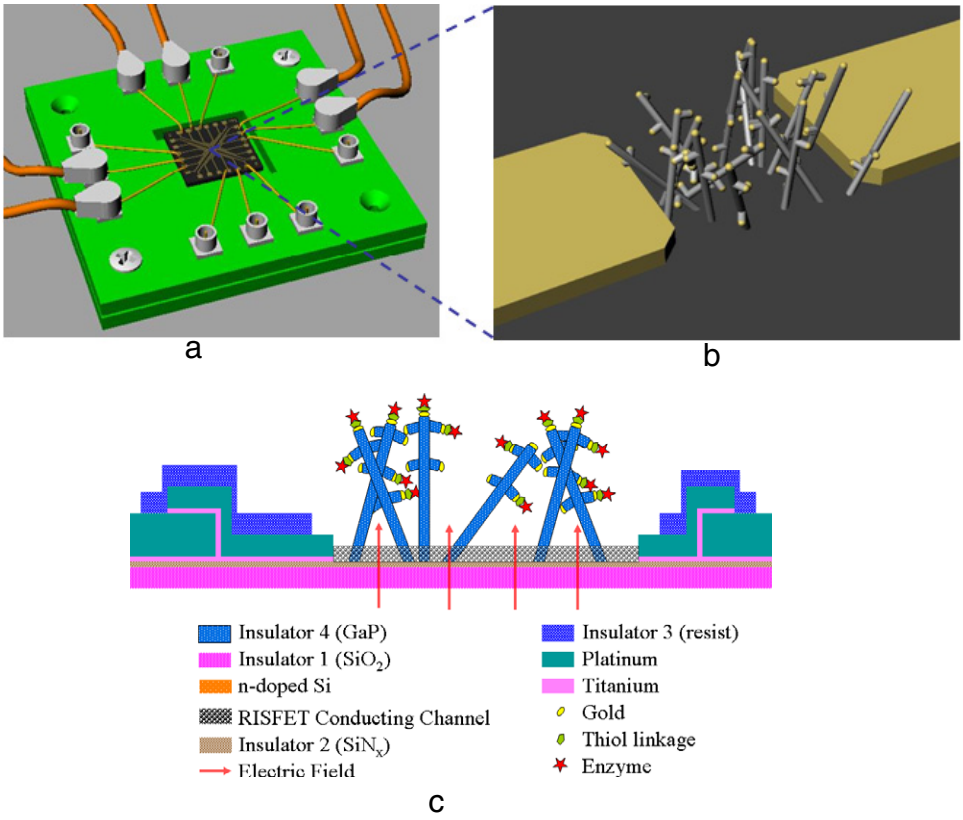

Figure 3. Schematic illustrations showing (a) a RISFET sensor chip inserted in a probe station with mini coax connections, (b) a future RISFET-based biosensor chip with a nanotree-based nanoreactor between the RISFET sensing electrodes, and (c) illustration of the conducting channel in a nanotree-based RISFET biosensor chip. The principle behind the RISFET sensor involves the on chip concentration of an analyte (or a product generated from the analyte enzymatically). The analyte (or product) is focused by a charged field to become concentrated in a narrow region—a conducting channel—located between two sensing electrodes. The focusing process leads to significant changes in conductivity, increasing the level of the current between the sensing electrodes and the ability to sense extremely low concentrations of specific analytes by means of an amplifying process.

showed that electric field strengths less than 1 MV m^{-1} do not affect the activity of the enzyme.

One issue in the development of multiple analyte nanobiosensor arrays is the development of suitable and addressable analyte-accessible nanoreactors. The complex nanorod structures (nanotrees) appeared to be a suitable enzyme matrix for lab-on-a-chip enzyme immobilization. Arrays of the proposed nanotree-based RISFET nanobiosensor have the potential for multianalytical pesticide field detection. Such devices would require low sample volume, and produce minimal waste. Moreover RISFET nanosensors have previously been shown to be highly sensitive and capable of analyzing pesticides down to about 20 ng l^{-1} [26].

3. Materials and methods

3.1. Biochemical material and methods

The enzymes acetylcholine esterase (AcChE), type VI-S, from Electric Eel (480 U mg^{-1} solid, 530 U mg^{-1} protein), Peroxidase Type VI from Horseradish (298 U mg^{-1} solid), and Choline oxidase from *Alcaligenes* species (16 U mg^{-1} solid) as well as acetylcholine chloride were purchased from Sigma Chemical Company, USA. 11-Mercapto undecanoic acid (MUA) was purchased from Aldrich. *N*-ethyl-*N*′-(3-dimethyl aminopropyl)-carbodiimide hydrochloride (EDC) and *N*-hydroxysuccinimide (NHS) were purchased from Sigma USA. TRIS base was purchased from Calbiochem®, Sweden. Acetonitrile (HPLC grade) was purchased from Labscan, Dublin, Ireland. Chemiluminescent substrate, Supersignal ELISA Pico was procured from Pierce USA. Hepes-buffered saline (HBS-EP) pH 7.4 was supplied in filtered and degassed form by BIAcore AB (Uppsala, Sweden). Chemiluminescence observations was performed on a 384 well plate (Nunc, Danmark) using a charge coupled device camera (Orca ER, Hamamatsu Photonics).

Water was purified (18.2 MΩ) by an Elgastat Maxima Apparatus (Elga Ltd, Bucks, England). TRIS/HCl buffer solution (1 mM, pH 7.4) was prepared using ultrapure water. Acetylcholine chloride (100 mM) was prepared using 1 mM TRIS/HCl pH 7.4. Prior to the experiment, a stock AcChE solution (2 U ml^{-1}) was prepared in TRIS/HCl buffer solution. HBS-EP buffer was used for the coupling reaction. N_2 gas of chemical grade (99.9996%) was supplied by Linde Gas Therapeutics, Sweden. All other chemicals used were of analytical grade.

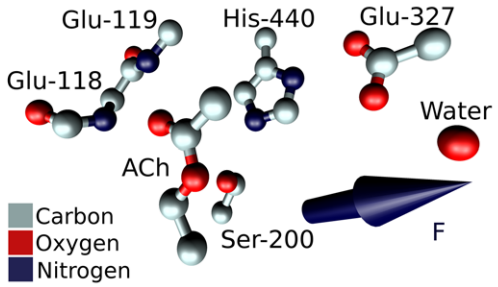

Figure 4. The active site model used in the density functional theory calculations without hydrogen atoms. The arrow represents the electric field vector (F) used in the calculations.

3.2. Nanostructure growth

GaP nanotrees were grown by sequential GaP nanorod growth, seeded by Au aerosol nanoparticles produced by an evaporation/condensation procedure [38]. For this technique, high-purity Au metal was heated in a tube furnace to 1850 °C to achieve an appropriate vapor pressure, then flushed from the furnace using ultrapure nitrogen gas, causing the rapid formation of gas phase Au nanoparticles by homogeneous nucleation. These particles were then charged with a β-Ni source to yield primarily singly-charged particles, then size-selected using a differential mobility analyzer (DMA) [39]. The flow density of the resulting monodisperse aerosol was measured by an electrometer, and particles were deposited onto the desired substrates via an electrostatic precipitator (ESP) [40]. For first-generation GaP nanorods, 40 nm aerosol nanoparticles with a surface density of 0.5 particles μm^{-2} were used; for second-generation rods (branches), 20 nm particles with a surface density of 10 μm^{-2} were deposited onto the first-generation rods. GaP substrates were used, as well as n-doped Si substrates thermally coated with a 100 nm SiO_x layer and a subsequent 30 nm SiN_y layer.

The two generations of nanorods were grown by low-pressure metal-organic vapor phase epitaxy (LP-MOVPE) at 10 kPa, in a 6 l min^{-1} flow of hydrogen gas. Substrates were first annealed at 650 °C for 10 min, to desorb any residual surface oxides (from the GaP substrates) as well as any organic contamination. Following this the temperature was reduced to 440 °C. Flows of the trimethylgallium (TMG, molar fraction 7.8×10^{-6}) and phosphine (PH_3, molar fraction 7.5×10^{-3}) were turned on to initiate growth. The growth time for first-generation rods was fixed at 60 or 120 s, while the branch growth time was 30 s.

3.3. Functionalization of the chip

The chips, with the nanorod and nanotree structures, were rinsed with ethanol and dried under nitrogen. A 1 mM solution of 11-mercaptothiol was prepared in ethanol. The chips were then incubated in the thiol solutions for 36 h in separate containers, backfilled with dry nitrogen. The chips were rinsed with ethanol two to three times and then sonicated for 2 min under the ethanol. The thiol self-assembly was activated by applying the EDC/NHS for 45 min at room temperature. The chip was rinsed with buffer to remove excess reagent. Subsequently AcChE (2 U ml^{-1}) HBS-EP buffer solution was incubated onto the chip for 2 h at room temperature. After the incubation, the chips were washed with buffer several times and stored under buffer for characterization of the immobilized enzyme. The thiol group binds to the gold supports [31], which are separated three dimensionally on the chip as caps on the tips of the nanorods and nanotree branches. EDC converts the carboxylic acid of the alkanethiol into reactive intermediates (NHS esters), which react with the free amine groups of the AcChE enzyme. The enzyme thus remains immobilized.

As a control experiment, another set of chips were non-specifically functionalized through adsorption of AcChE on the chip. The enzyme solution (2 U ml^{-1} stock) was incubated on the surface of the chip for 3–4 h at room temperature (26 °C). After 4 h, the chip was rinsed with the buffer solution several times. Acetylcholine was added onto the chip, following the procedure applied for the thiol-functionalized chip. Tests were also performed on thiolated surfaces not activated by EDC.

3.4. Characterization

The morphology of the nanostructures grown at different substrates was investigated using a scanning electron microscope (SEM) at 18 kV, using a dual beam focused ion beam (FIB)/SEM-FEI NanoLab 600, from FEI Company, USA.

The chips with the functionalized AcChE enzyme, as well as the control samples, were characterized using chemiluminescence measurements. In the actual setup, acetylcholine chloride AcChCl, (0.25 mM) was added to the chip (20 μl on chip active surface) and allowed to react. From this reaction, a 5 μl sample was taken out after 10 min (optimized time) to which Choline oxidase 0.01 U, HRP 0.001 U, and luminol 20 μl were added. The total assay volume was 30 μl in a 384 well plate format. The photons were counted and imaged using a charge coupled device camera. The assay buffer was TRIS/HCl (pH 7.4). The experiments for the functionalized long nanorods and the functionalized branched nanotrees were conducted within the same batch of samples.

3.5. Quantum chemical calculations

Calculations were performed with density functional theory, using the B3LYP functional [35, 41], as implemented in the Turbomole software [42]. These calculations employed the 6-31G* basis set for all atoms. Structures were optimized until the change in energy between two iterations was below 2.6 J mol^{-1} (10^{-6} au) and the maximum norm of the internal gradients was below 10^{-3} au.

To model the active site we used the crystal structure of an acetylcholine esterase from *Torpedo californica*, taken from the Protein Data Bank (entry 2ACE) [43]. In our calculations, as is shown in figure 4, Ser-200 is represented by ethanol, His-440 by a methyl imidazole ring, Glu-327 by an acetate anion complexed with a water molecule, the oxyanion hole (Glu-118 and Glu-119) by a dipeptide-like structure $CH_3NHCOCH_2NHCHO$, and AcCh by $CH_3COOC_2H_5$. This

model has previously been shown to give an accurate description of the reactivity [44].

After adding protons, the water molecule, and the substrate model to the crystal structure, a geometry optimization with the atoms available in the crystal structure were kept fixed. Then, a new geometry optimization was performed with all atoms free to move, resulting in the final geometry of the reactant state. After this, a scan of the distance between the Ser-200 oxygen atom and the reacting carbon of the substrate was performed from 3.5 to 1.5 Å. The transition state and the product state were optimized without any constraints from the 1.7 Å and 1.5 Å structures, respectively.

Acknowledgments

The authors thank Fredrik Pontén and Thomas Andén for their contribution to the color artwork. Part of this work was performed within the Nanometer Structure Consortium at Lund University. Financial support from the Swedish Foundation for Strategic Research (SSF), the Swedish Research Council (VR; Contracts nos 230-2000-340 and 621-2001-2753), as well as the Benzon foundation is gratefully acknowledged.

References

[1] Newman J D, Tigwell L J, Warner P J and Turner A P F 2001 Biosensors: boldly going into the new millennium *Sensor Rev.* **21** 268–71

[2] Xie B and Danielsson B 1996 An integrated thermal biosensor array for multianalyte determination demonstrated with glucose, urea and penicillin *Anal. Lett.* **29** 1921–32

[3] Xie B, Ramanathan K and Danielsson B 2000 Mini/micro thermal biosensors and other related devices for biochemical/clinical analysis and monitoring *TRAC Trends Anal. Chem.* **19** 340–9

[4] Karube I and Yokoyama K 1993 Trends in biosensor research and development *Sensors Actuators* B **13** 12–5

[5] de Souza P R 2000 Detection of the absorption of glucose molecules by living cells using atomic force microscopy *FEBS Lett.* **475** 43–6

[6] Vo-Dinh T 2002 Nanobiosensors: probing the sanctuary of individual living cells *J. Cell. Biochem.* **87** 154–61

[7] Klemic J F, Stern E and Reed M A 2001 Hotwiring biosensors *Nat. Biotechnol.* **19** 924–5

[8] Reimhult K, Yoshimatsu K, Risveden K, Chen S, Ye L and Krozer A 2008 Characterization of QCM sensor surfaces coated with molecularly imprinted nanoparticles *Biosens. Bioelectron.* **23** 1908–14

[9] Ji T, Rai P, Jung S and Varadan V K 2008 *In vitro* evaluation of flexible pH and potassium ion-sensitive organic field effect transistor sensors *Appl. Phys. Lett.* **92** 233304

[10] Cui Y, Wei Q, Park H and Lieber C M 2001 Nanowire nanosensors for highly sensitive and selective detection of biological and chemical species *Science* **293** 1289–92

[11] Chiragwandi Z G, Nur O, Willander M and Calander N 2003 DC characteristics of a nanoscale water-based transistor *Appl. Phys. Lett.* **83** 5310–2

[12] Alivisatos P 2004 The use of nanocrystals in biological detection *Nat. Biotechnol.* **22** 47–52

[13] Bi X, Wong W L, Ji W, Agarwal A, Balasubramanian N and Yang K-L 2008 Development of electrochemical calcium sensors by using silicon nanowires modified with phosphotyrosine *Biosens. Bioelectron.* **23** 1442–8

[14] Bi X, Agarwal A, Balasubramanian N and Yang K-L 2008 Tripeptide-modified silicon nanowire based field-effect transistors as real-time copper ion sensors *Electrochem. Commun.* **10** 1868–71

[15] Tierney M J, Tamada J A, Potts R O, Jovanovic L and Garg S 2001 Cygnus research team. clinical evaluation of the GlucoWatch® biographer: a continual, non-invasive glucose monitor for patients with diabetes *Biosens. Bioelectron.* **16** 621–9

[16] Cavalcanti A, Shirinzadeh B, Zhang M J and Kretly L C 2008 Nanorobot hardware architecture for medical defense *Sensors* **8** 2932–58

[17] Bi X, Agarwala A, Balasubramaniana N and Yangb K-L 2008 Tripeptide-modified silicon nanowire based field-effect transistors as real-time copper ion sensors *Electrochem. Commun.* **10** 1868–71

[18] Patolsky F, Timko B P, Yu G, Fang Y, Greytak A B, Zheng G and Lieber C M 2006 Detection, stimulation, and inhibition of neuronal signals with high-density nanowire transistor arrays *Science* **313** 1100–4

[19] Risveden K and Danielsson B 2005 Nanoscale dielectrophoresis as a tool for studies of single biomolecules in aqueous environment: water transistor based NANOSENSOR *Keynote Lecture SMCBS 2005: The 2nd Int. Workshop on Surface Modification for Chemical and Biochemical Sensing (Polen, Kazimierz Dolny, Nov. 2005)*

[20] Risveden K, Pontén J F, Calander N, Willander M and Danielsson B 2006 The region ion sensitive field effect transistor, a novel bioelectronic nanosensor *Proc., the XX Eurosensors, 20th Anniversary (Göteborg 2006)* vol II pp 440–1

[21] Risveden K, Pontén J F, Calander N, Willander M and Danielsson B 2007 The region ion sensitive field effect transistor, a novel bioelectronic nanosensor *Biosens. Bioelectron.* **22** 3105–12

[22] Stern E, Klemic J F, Routenberg D A, Wyrembak P N, Turner-Evans D B, Hamilton A D, LaVan D A, Fahmy T M and Reed M A 2007 Label-free immunodetection with CMOS-compatible semiconducting nanowires *Nature* **445** 519–22

[23] Stern E, Vacic A and Reed M A 2008 Semiconducting nanowire field-effect transistor biomolecular sensors *IEEE Trans. Electron. Devices* **55** 3119–30

[24] Montelius L, Tegenfeldt J O and Ling T G I 1995 Fabrication and characterization of a nanosensor for admittance spectroscopy of biomolecules *J. Vac. Sci. Technol.* A **13** 1755–60

[25] Montelius L, Tegenfeldt J O and Ling T G I 1995 A nanosensor for admittance spectroscopy. In the ultimate limits of fabrication and measurements *Proc. NATO Advanced Research Workshop (Cambridge, Apr. 1994)* ed M E Welland and J K Gimzewski (Berlin: Springer) pp 115–22

[26] Risveden K, Bhand S, Pontén J F, Andén T, Calander N, Willander M and Danielsson B 2007 Signal frequency studies of an environmental application of a 65 nm region ion sensitive field effect transistor sensor *Sensors Actuators* B **127** 198–203

[27] Risveden K 2008 *Bioelectronic Nanosensor Devices for Environmental and Biomedical Analysis* (Lund: Tryckeriet I E-huset, Lund University) ISBN 978-91-628-7421-6

[28] Chirgwandi Z G, Panas I, Johansson L-G, Norden B, Willander M, Winkler D and Agren H 2008 Properties of a biophotovoltaic nanodevice *J. Phys. Chem.* C **112** 18717–21

[29] Thelander C *et al* 2006 Nanowire-based one-dimensional electronics *Mater. Today* **10** 28–35

[30] Dick K A 2008 A review of nanowire growth promoted by alloys and non-alloying elements with emphasis on Au-assisted III–V nanowires *Prog. Cryst. Growth Charact. Mater.* **54** 138–73

[31] Meng Q, Mecklenburg M, Danielsson B, Risveden K and Xie B 2004 Development of a tRNA-synthetase microarray for protein analysis *Sensors Mater.* **16** 401–12
[32] Dick K A, Deppert K, Mårtensson T, Seifert W and Samuelson L 2006 Growth of GaP nanotree structures by sequential seeding of 1D nanowires *J. Cryst. Growth* **272** 131–7
[33] Mårtensson T, Svensson C P T, Wacaser B A, Larsson M W, Seifert W, Deppert K, Gustafsson A, Wallenberg L R and Samuelson L 2004 Epitaxial III–V nanowires on Si *Nano Lett.* **4** 127–32
[34] Dick K A, Deppert K, Karlsson L S, Larsson M W, Seifert W, Wallenberg L R and Samuelson L 2007 Directed growth of branched nanowires structures *MRS Bull.* **32** 127
[35] Hertwig R H and Koch W 1997 On the parameterization of the local correlation functional. What is Becke-3-LYP? *Chem. Phys. Lett.* **268** 345–51
[36] Svitel J, Dzgoev A, Ramanathan K and Danielsson B 2000 Surface plasmon resonance based pesticide assay on a renewable biosensing surface using the reversible concanavalin A monosaccharide interaction *Biosens. Bioelectron.* **15** 411–5
[37] Svitel J, Surugiu I, Dzgoev A, Ramanathan K and Danielsson B 2001 Functionalized surfaces for optical biosensors: applications to *in vitro* pesticide residual analysis *J. Mater. Sci.* **12** 1075–8
[38] Magnusson M H, Deppert K, Malm J-O, Bovin J-O and Samuelson L 1999 Gold nanoparticles: production, reshaping, and thermal charging *J. Nanopart. Res.* **1** 243–51
[39] Knutson E O and Whitby K T 1975 Aerosol classification by electric mobility: apparatus, theory, and applications *J. Aerosol Sci.* **6** 443–51
[40] Deppert K, Schmidt F, Krinke T, Dixkens J and Fissan H 1996 Electrostatic precipitator for homogeneous deposition of ultrafine particles to create quantum-dot structures *J. Aerosol Sci.* **27** 151–2
[41] Becke A D 1993 A new mixing of Hartree–Fock and local density-functional theories *J. Chem. Phys.* **98** 1372–7
[42] Treutler O and Ahlrichs R 1995 Efficient molecular numerical integration schemes *J. Chem. Phys.* **102** 346–54
[43] Raves M L, Harel M, Pang Y-P, Silman I, Kozikowski A P and Sussman J L 1997 Structure of acetylcholinesterase complexed with the nootropic alkaloid, (-)-huperzine A *Nat. Struct. Biol.* **4** 57–63
[44] Manojkumar T K, Cui C and Kim K S 2004 Theoretical insights into the mechanism of acetylcholinesterase-catalyzed acylation of acetylcholine *J. Comput. Chem.* **26** 606–11